Morphological Behavior Bridging the Symmetric AB and ABC States in the Poly(styrene-*b*-isoprene-*b*-ethylene oxide) Triblock Copolymer System

Travis S. Bailey, Hoai D. Pham, and Frank S. Bates*

Department of Chemical Engineering and Materials Science, University of Minnesota, Minneapolis, Minnesota 55455

Received February 23, 2001; Revised Manuscript Received July 9, 2001

ABSTRACT: We report on the characterization of the morphological behavior expressed between the symmetric AB diblock and ABC triblock copolymer states. Experimentally, a gradual transformation between these states was achieved through systematic addition of PEO to a single symmetric PS−PI diblock copolymer (MW ∼ 18 800 g/mol), resulting in a series of 10 poly(styrene-*b*-isoprene-*b*-ethylene oxide) triblock copolymers varying only in the amount of PEO added. Final compositions ranged from 2.9 to 33.2 vol % (experimentally symmetric) PEO, with the remaining volume necessarily divided equally between the PS and PI segments. The molecular weight of the parent diblock was chosen such that resulting triblocks would undergo order−disorder transitions (ODTs) at experimentally accessible temperatures over much of the composition range studied. Our results focus on the detection and characterization of six morphologies observed to form between these two symmetric states and some of the kinetic and directional (heating vs cooling) characteristics of two thermally induced order−order transitions (OOTs) observed. We conclusively identify the formation of two- and three-domain lamellar structures, hexagonally packed core−shell cylinders, and the pentacontinuous core−shell gyroid morphology and speculate on probable assignments for two untypical structures also observed. Finally, we discuss some of the general behavior characteristics of this system in terms of their dependence on block connectivity and χ interaction parameter sequencing.

Introduction

When compared to their AB counterparts, ABC type block copolymers offer an increased potential to create systems with tailored chemical, physical, and mechanical properties and functions.[1,2] Their attractiveness lies in the unique and complex morphologies they express, with multiple levels of domain co-continuity possible. Many unique morphologies, in several ABC systems, have been observed and reported over the past decade;[3−11] however, a thorough understanding of phase behavior in any one ABC system has yet to be realized. With the exception of those mentioned above and several others,[12−14] systematic investigations of morphological behavior with respect to changes in composition, block sequence, molecular weight, and temperature are limited. Consequently, knowledge of ABC phase behavior is generally restricted to very small ranges of composition over an assortment of chemically distinct systems. This curt treatment is largely a result of the demanding synthesis and rigorous characterization techniques required to investigate any ABC system at even a single composition, with study of multiple compositions proving extremely severe. In addition, most investigations to date have dealt with systems of significant segregation strength,[3−11,13,14] where thermal dependence of the morphological behavior is rarely a consideration and realization of a true equilibrium state is frequently suspect. Working with systems in the intermediate and weakly segregated regimes where the disordered state is experimentally accessible improves the potential to address these problematic details, a strategy used previously in the general characterization of AB diblock copolymer systems.[15,16] It also has been observed in AB systems that complex morphological behavior is largely limited to more weakly segregated states, where formation of the bicontinuous gyroid structure as well as thermally dependent order−order transitions (OOTs) have been reported.[15−20] In consideration of these issues, we were motivated to investigate the morphological behavior in a single ABC system over a significant composition range, on weakly segregated molecules in the vicinity of their order−disorder transitions (ODTs).

To this end, a sequence of 10 poly(styrene-*b*-isoprene-*b*-ethylene oxide) (PS−PI−PEO) triblock copolymers was synthesized from a single, *symmetric,* parent poly(styrene-*b*-isoprene) (PS−PI) diblock copolymer. Using this synthetic strategy, it was possible to create a sequence of triblock copolymers possessing only differences in the amount of poly(ethylene oxide) (PEO) contained in the molecule, the size and distribution of the polystyrene (PS) and polyisoprene (PI) segments being necessarily identical throughout the sequence (Figure 1). The PEO volume fraction was varied from zero to one-third, permitting the study of composition space between the symmetric AB and ABC block copolymer states (Table 1).

It should be emphasized that our incorporation of PEO as the final block in the sequence was not arbitrary. Reinitiation and subsequent growth of PEO from a hydroxyl functional macromolecule is extremely reliable and synthetically robust.[21] Growth of each triblock from a previously synthesized batch of parent diblock significantly reduces the synthetic demands typical of such a systematic investigation. In addition, by carefully choosing the molecular weight of the parent diblock copolymer, maintaining triblock copolymer ODTs in an experimentally viable temperature window was possible over much of the composition range studied. A final, but

* To whom correspondence should be addressed.

10.1021/ma0103371 CCC: $20.00
Published on Web 08/23/2001

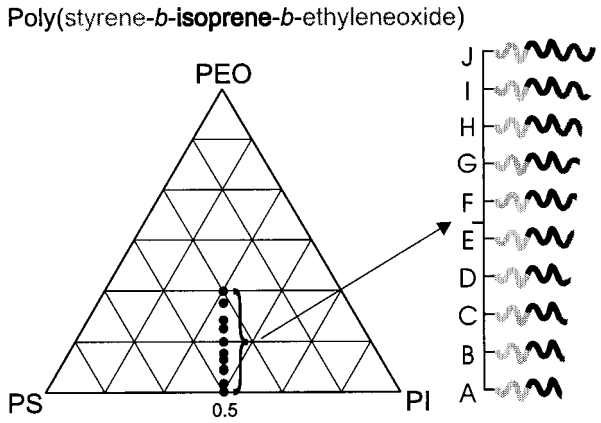

Figure 1. ABC ternary composition diagram showing the parent poly(styrene-*b*-isoprene)−OH diblock and 10 poly(styrene-*b*-isoprene-*b*-ethylene oxide) triblock copolymers characterized in this study.

Table 1

polymer	M_n[a]	polydispersity[b]	f_{PS} (±0.002)[c]	f_{PI} (±0.002)	f_{PEO} (±0.002)
parent diblock	18 760	1.04	0.497	0.501	0.002
triblock A (SIO2)	19 370	1.08	0.483	0.488	0.029
triblock B (SIO4)	20 450	1.07	0.462	0.466	0.072
triblock C (SIO1)	20 530	1.07	0.460	0.464	0.076
triblock D (SIO5)	21 390	1.08	0.444	0.448	0.108
triblock E (SIO3)	21 960	1.09	0.434	0.438	0.128
triblock F (SIO6)	23 110	1.11	0.415	0.419	0.166
triblock G (SIO7)	24 580	1.10	0.394	0.397	0.209
triblock H (SIO8)	25 580	1.11	0.380	0.383	0.237
triblock I (SIO9)	27 880	1.12	0.352	0.355	0.293
triblock J (SIO10)	29 680	1.11	0.333	0.335	0.332

[a] In g/mol (±100 g/mol). Determined by ^{1}H NMR and MALDI-TOF mass spectrometry of parent diblock. [b] Determined using polystyrene standards in $CHCl_3$. [c] Volume fractions were calculated based on densities reported at 140 °C by Fetters et al.[32] (ρ_{PS} = 0.969 g/cm^3, ρ_{PI} = 0.830 g/cm^3, ρ_{PEO} = 1.064 g/cm^3).

not insignificant, consideration was the potential role of complex morphological structures in the pursuit of improved ionic conduction membranes. Our goal was to create a PEO-containing ABC system capable of self-assembly into structures with different extents of co-continuity (including the core−shell pentacontinuous gyroid morphology).[4] Incorporation of ionic salts into PEO domains while maintaining morphological structure would be an achievement greatly beneficial to this area of research and is currently being investigated on the basis of the results reported here.

In addition to presenting detailed analysis of the morphological structures and transitions encountered across this composition range, we also attempt to understand the energetic forces driving the observed progression as we travel from one symmetric state to the other. Our discussion focuses on the potential discrepancy between the two interfaces *required* by the architectural constraints of the system and the two that would be enthalpically *preferred* in their absence. This discrepancy or "frustration" condition in ABC systems is typically discussed in terms of the relative values of the Flory−Huggins segment−segment interaction parameter χ, a measure of the enthalpic penalty incurred for contact between dissimilar pairs of polymers.[22,23] For this particular system, $\chi_{PI/PEO}$ is much larger than either $\chi_{PS/PEO}$ or $\chi_{PS/PI}$, and so frustration arises as a result of the covalent linkage forcing an interface between the two blocks with the largest energetic penalty for contact (PI and PEO).[24] The consequence of such sequencing is the predisposition of a system to form a third interface between the noncovalently linked segments. The actual formation of this third interface is of course limited to cases where the overall free energy is reduced, despite the entropic stretching penalties typically incurred as a result of its formation. Careful balancing of the energies associated with frustrated systems has been credited with the formation of various complex structures, including spheres on spheres, rings on cylinders, cylinders at lamellar interfaces, spheres at lamellar interfaces, and the notable knitting pattern morphology to name a few.[6,8,9,25] In fact, we believe the formation of two of the morphologies observed in this study can also be understood as a consequence of frustration inherent to the PS−PI−PEO system.

Evaluation of the morphological and thermal behavior of the PS−PI−PEO triblock copolymer sequence was performed using a collection of analytical techniques. Simple rheological measurements of the elastic and loss moduli were used to establish basic trends in the thermal behavior, such as order−disorder[26] and possible order−order[27,28] transitions. Small-angle X-ray scattering (SAXS) was used to establish the scattering signatures of each triblock as a function of temperature. These data were then used to verify the ODTs and OOTs suggested by the rheological measurements. In many cases, identification of the morphological structure was possible from SAXS measurements alone, when Bragg peak assignment and spatial domain arrangement were conclusive. In cases where SAXS data were ambiguous, supportive visual evidence was obtained through transmission electron microscopy (TEM) performed on samples in which trapping of the melt state morphological structure at room temperature was possible. Selective staining in samples investigated by TEM was used to elucidate both morphological structure and specific domain placement within a particular morphology.

To obtain a greater understanding of the boundary locations between morphological regions, SAXS data were collected on blends of consecutive pairs of triblocks in the sequence (Figure 1). By investigating these blends, it was possible to approximate the behavior of molecules with volume fractions of PEO falling between those of the triblock pair. Remarks concerning the merits of data approximated through blending in this manner are saved for the Discussion section of this article. Finally, boundaries defining thermally induced OOTs were probed using a combination of rheology and SAXS measurements, in an effort to better understand the kinetic and directional (heating vs cooling) characteristics of these transitions.

Experimental Section

Synthesis of Hydroxyl-Terminated Poly(styrene-*b*-isoprene) Diblock Copolymer Precursor. Synthesis of this parent molecule was achieved through sequential anionic polymerization of styrene and isoprene, followed by end-capping with ethylene oxide (one unit) to generate the polymeric alcohol. Purification of styrene, isoprene, ethylene oxide, and cyclohexane has been described previously.[21,29] Styrene was initiated by *sec*-butyllithium under an argon atmosphere and polymerized at 40 °C in cyclohexane. This was followed by isoprene addition, also polymerized at 40 °C (∼95% 1,4 addition). Subsequent addition of ethylene oxide (5−15 × [Li^+]) resulted in the incorporation of a single $-CH_2CH_2O-$ unit to each polymer chain, a consequence of reduced nucleophilicity of the oxanionic species in the presence of lithium cations.[30,31] Termination with acidic methanol (HCl) was used to liberate

the final hydroxyl-terminated diblock copolymer. Residual acid and salts were removed through multiple washes with sodium bicarbonate solution followed by water. Recovery was achieved through precipitation into a 3:1 solution of methanol and 2-propanol, followed by multiple washes with methanol, filtration, and complete drying under dynamic vacuum.

Synthesis of Poly(styrene-*b*-isoprene-*b*-ethylene oxide) Triblock Copolymers. Synthesis of all triblock species was achieved through reinitiation of the terminal hydroxyl group of the parent diblock, followed by the controlled propagation of ethylene oxide monomer. A measured amount of hydroxyl-terminated parent diblock copolymer was dissolved in tetrahydrofuran under an argon atmosphere and subsequently titrated to the potassium alkoxide by a solution of potassium naphthalenide in tetrahydrofuran. Details concerning the preparation of the titrating solution and this general procedure have been described by Hillmyer et al.[21] The titrating solution's dark green color disappears upon formation of the potassium alkoxide, and thus a residual green tint in the polymer solution was used as evidence that all hydroxyl species had reacted and the end point had been reached. Note that naphthalene and dihydronaphthalene are byproducts of this titration and are removed during the final drying of the polymer product. Addition of ethylene oxide following the titration results in chain propagation; the oxanion nucleophilicity now increased in the presence of potassium counterions. Acidic methanol was again used to terminate the final triblock copolymer, which was then redissolved into dichloromethane after removal of the tetrahydrofuran by rotary evaporation. The solution was washed multiple times with saturated sodium bicarbonate solution followed by distilled water. The dichloromethane was then removed by rotary evaporation and the final product freeze-dried from benzene under dynamic vacuum.

Chemical Characterization. Molecular weight distributions and polydispersity for all samples were obtained by gel permeation chromatography (GPC) on a Waters 150-C ALC/GPC. All samples were run in chloroform at 25 °C on Phenomenex Phenogel columns. Polystyrene standards from Polymer Laboratories were used as a basis for polydispersity calculations (Table 1). Samples with more than 3% residual parent diblock copolymer were excluded from this investigation. In most samples, residual parent diblock was essentially undetectable, underscoring the efficiency of the diblock endcapping and subsequent reinitiation steps.

Fractional composition was determined using ^{1}H NMR on a Varian 300 MHz instrument, with all samples dissolved in deuterated chloroform. Delay times between acquisitions were set to 30 s to allow for required sample relaxation. Block mole fractions were determined using relative integrated peak intensities and converted to volume fractions using published homopolymer densities reported at 140 °C.[32] Note that these nominal densities are arbitrarily chosen, and data reported here are not corrected for relative changes that occur as a function of temperature.

Molecular weights of triblock copolymers A−J were inferred from ^{1}H NMR and the parent diblock molecular weight, which was determined independently by MALDI-TOF mass spectroscopy. Mass spectroscopy was performed by the University of Minnesota Chemistry Department, using a Bruker Daltonics Reflex III mass spectrometer. Samples were run in a linear mode at 20 kV using a dithranol matrix with Ag^+ cation. Chemical characterization results for all copolymers are listed in Table 1.

Rheology. All rheological measurements were performed using a Rheometrics Scientific dynamic stress rheometer or the Rheometrics Scientific ARES rheometer, both in the 25 mm diameter, parallel-plate configuration. Measurements of elastic and loss moduli were obtained as a function of increasing temperature at a constant ramp rate (heating and cooling) of 1 °C/min (unless otherwise stated), under a constant blanket of pure nitrogen gas. A strain range was carefully chosen for each sample such that measurements over the entire temperature range were maintained in the linear viscoelastic region of the material, although typically held between 0.5 and 1.0%. The stress applied to the sample was varied to stay within the limits of this strain range. All investigations to determine ODTs were run from 70 °C up to temperatures 15 °C beyond the point of disorder in the sample, defined by a sudden decrease in the elastic modulus to below 1.0 Pa. In samples where more complex rheological behavior was detected (OOTs), more rigorous probing of the transition areas was performed; however, the conditions of these experiments are discussed in combination with their results in the main text of this article.

Samples for investigation were prepared as 1.25 mm thick films 25.0 mm in diameter. Films were formed from powders placed in a mold and subsequently hot pressed at 500 psi for 5−7 min. Samples were pressed at temperatures approximately 15 °C below the ODT and then annealed on the rheometer just above but as close to the ODT as possible for 10 min prior to cooling to the starting temperature of 70 °C. It should be noted that the error in the temperatures of the hot press are easily ±5 °C. Confirmation of order−disorder and order−order transitions suggested by the rheological measurements was made through comparison with SAXS data. Note that rheological measurements on "blindly" prepared samples were used to estimate ODTs for final sample preparation temperatures on repeated experiments.

Small-Angle X-ray Scattering (SAXS). SAXS measurements were made at the Institute of Technology (IT) characterization facility at the University of Minnesota. Copper Kα radiation (wavelength = 1.54 Å) was generated by a Rigaku Ru-200BVH rotating anode using a 0.2 × 2.0 mm^2 microfocus cathode and monochromatized by total reflecting Franks mirrors and a nickel foil filter. Two-dimensional scattering data were collected by a Siemens HI-STAR multiwire area detector. All data were corrected for detector response characteristics prior to analysis. Samples were run under a vacuum atmosphere of several Torr. All SAXS data presented in this article are plotted on a logarithmic intensity scale as a function of the magnitude of the scattering vector q, defined by $q = (4\pi/\lambda)\sin(2\theta/2)$, where 2θ is the angle between the incident and scattered radiation. The two-dimensional data presented here have been azimuthally integrated for convenience of presentation; however, all data were isotropic in the 2-D form. Samples of pure triblock were prepared by sealing powder in 2.0 mL ampules under vacuum and then annealing as described in Table 2. Blended samples of consecutive triblock pairs were prepared by solution blending in benzene followed by subsequent freeze-drying directly in a 2 mL ampule. Ampules were then sealed under vacuum, and the dried sample annealed as reported in Table 2. It is important to note that pure triblocks were also subjected to freeze-drying from benzene as the last step of the purification process described above.

Transmission Electron Microscopy (TEM). TEM images were also obtained at the IT characterization facility at the University of Minnesota, using a JEOL 1210 TEM operating at 120 kV. Thin film samples were prepared using a Reichart ultramicrotome mounted with a Microstar diamond knife. Samples generally were cut between −65 and −40 °C and placed on 400 mesh copper grids (Ted Pella). Contrast within the sample was achieved through selective staining of the PI domains using vapor from a 4% aqueous solution of osmium tetroxide (Ted Pella). Samples were exposed to the vapor for between 2 and 5 min.

Films of triblocks and the parent diblock were prepared for microtoming according to the temperature schemes described in Table 2. In general, the films were annealed in the melt state for long times (ca. 50−75 h) before lowering the temperature to 80 °C for additional time. The purpose of this strategy was to "trap" the melt morphology using the glassy state of the PS domains (below 100 °C), prior to cooling rapidly (30 °C/min) to room temperature (20 °C). It was observed that following this strategy we could maintain the melt morphology adequately and avoid possible disruption of the lattice by crystallization in the PEO domains occurring below 65 °C. Confirmation of a "trapped" morphology was easily made by comparison of SAXS data of the newly formed samples (at room temperature) with that observed for the melt state.

Table 2

polymer	f_{PEO}	annealing for SAXS: temp 1 (°C) (5 min)	annealing for SAXS: temp 2 (°C)	annealing for TEM: temp 1 (°C)	annealing for TEM: temp 2 (°C)	annealing for TEM: temp 2 (°C)	morphological behavior
parent diblock	0.002	125	77 (72 h)	130 (30 min)	105 (72 h)	80 (120 h)	$LAM_2 \rightarrow DIS$
blend DB/A-1	0.015	125	77 (72 h)				$LAM_2 \rightarrow DIS$
triblock A	0.029	125	77 (72 h)				$LAM_2 \rightarrow DIS$
blend A/B-1	0.043	125	77 (72 h)				PLS → DIS
blend A/B-2	0.058	125	77 (72 h)				PLS → DIS
triblock B	0.072	125	77 (72 h)				PLS → DIS
triblock C	0.076	130	105 (36 h)	130 (30 min)	105 (72 h)	80 (72 h)	PLS → DIS
blend C/D-1	0.086	165	105 (26 h)				CSC → PLS → DIS
blend C/D-2	0.097	165	105 (26 h)				CSC → DIS
triblock D	0.108	165	135 (36 h)				CSC → DIS
triblock E	0.128	180	130 (48 h)				CSC → DIS
triblock F	0.166	200	135 (36 h)	225 (30 min)	160 (50 h)	80 (72 h)	CSC → DIS
blend F/G-I	0.180	225	175 (42 h)				CSC → DIS
blend F/G-2	0.195	225	175 (42 h)				CSG → CSC → DIS
triblock G	0.209	225	165 (24 h)	225 (30 min)	160 (50 h)	80 (72 h)	CSG → CSC → DIS
blend G/H-1	0.218	225	175 (42 h)				CSG → CSC → DIS
blend G/H-2	0.228	225	175 (42 h)				CSG → CSC →
triblock H	0.237	225	200 (12 h)	225 (30 min)	180 (63 h)	80 (120 h)	SPL → CSC →
blend H/I-1	0.251	225	185 (120 h)				$LAM_3 \rightarrow$ SPL → CSC →
blend H/I-2	0.265	225	185 (120 h)				$LAM_3 \rightarrow$ SPL →
blend H/I-3	0.279	225	185 (120 h)				$LAM_3 \rightarrow$ SPL →
triblock I	0.293	225	200 (12 h)				$LAM_3 \rightarrow$
blend I/J-I	0.312	225	185 (120 h)				$LAM_3 \rightarrow$
triblock J	0.332	225	200 (12 h)	225 (30 min)	180 (75 h)	80 (96 h)	$LAM_3 \rightarrow$

Results and Analysis

A combination of the parent PS−PI diblock, 10 PS−PI−PEO triblocks, and 13 blends of consecutive triblock pairs was used to investigate the phase behavior of the PS−PI−PEO system along the isopleth described by Figure 1. The PEO content was varied between 0 and 33.2 vol % along this isopleth, which maintains the ratio of PS to PI volumes at approximately 0.99 (equal volumes). A summary of the morphological behavior exhibited by this sequence of molecules and intermediate blends of consecutive pairs is depicted in Figure 2. The composition axis of this phase diagram simply describes the volume fraction of PEO in the molecule or blend, recognizing the remaining volume must be equally divided between the PS and PI segments. Investigation of the thermal dependence of the morphological behavior was limited by the crystallization temperature of PEO ($T_m \cong 65$ °C) and the maximum accessible temperature permitted by the SAXS instrument of 225 °C. Chemical degradation above this maximum temperature would be a serious consideration regardless. Four distinct morphologies were observed to separate the anticipated AB (two-domain) and ABC (three-domain) lamellar structures found to bracket this region of phase space. The progression of morphologies between these lamellar states (LAM_2 and LAM_3) includes a proposed pillared lamellar structure (PLS), hexagonally packed core−shell cylinders (CSC), the pentacontinuous core−shell gyroid morphology (CSG), and a tentatively assigned semiperforated lamellar structure (SPL), similar to the metastable perforated lamellar (PL) phase detected in several AB diblock copolymer systems.[15,16,18,20,27,33−35] Four OOTs were detected across the composition range studied, although two of the four were observed at PEO compositions represented only by intermediate blends. Transitions identified were between CSC and the proposed PLS (blends only), CSG and CSC, the suspected SPL and CSC, and the LAM_3 and the suspected SPL phase (blends only).

The development of Figure 2 was carried out through systematic characterization of the parent diblock and each triblock (A−J), acquiring rheology and SAXS data on each as a function of temperature. From rheological measurements, distinct changes in the elastic and loss moduli (G' and G'', respectively) were used to determine ODTs and OOTs for the various molecules, although all transitions were subsequently verified by corresponding changes in SAXS Bragg peak positions. The basic rheology traces for most samples have been omitted due to space limitations; however, examples of the data for triblocks G and H can be found in Figures 6 and 7. Hysteresis in most identified transitions was largely negligible, limited to only several degrees when rates were restricted to 1 °C/min. Slower rates diminished the hysteresis by increasing the temperature of the cooling transition, leaving the temperature of the heating transition essentially unchanged. Consequently, the values of the transition temperatures designated in Figure 2 were assigned from data collected while heating, the rate independence of these values suggesting they are more indicative of the actual transition temperatures. It is noted, however, that significant hysteresis and a large cooling rate dependence were found in one of the four OOTs observed in this study (CSC to CSG, triblock G), a matter that is addressed later in more detail. SAXS data collected provided not only verification of these transitions but, more importantly, structural information about the samples as well. In addition to the parent diblock and triblocks A−J, SAXS data were also collected on intermediate blends of consecutive triblock pairs. Using simply the uniqueness of the scattering profiles specific to particular regions, it was possible to outline a phase diagram with boundaries separating areas of structurally different morphologies. The intermediate blends were used to approximate these boundaries in the diagram more closely, avoiding additional rigorous synthesis of intermediate molecules. Unlike the parent diblock and triblocks A−J, rheological experiments on the blends were avoided due to the significant material requirements of this technique. As a result, ODTs and OOTs in the blended samples were simply estimated from

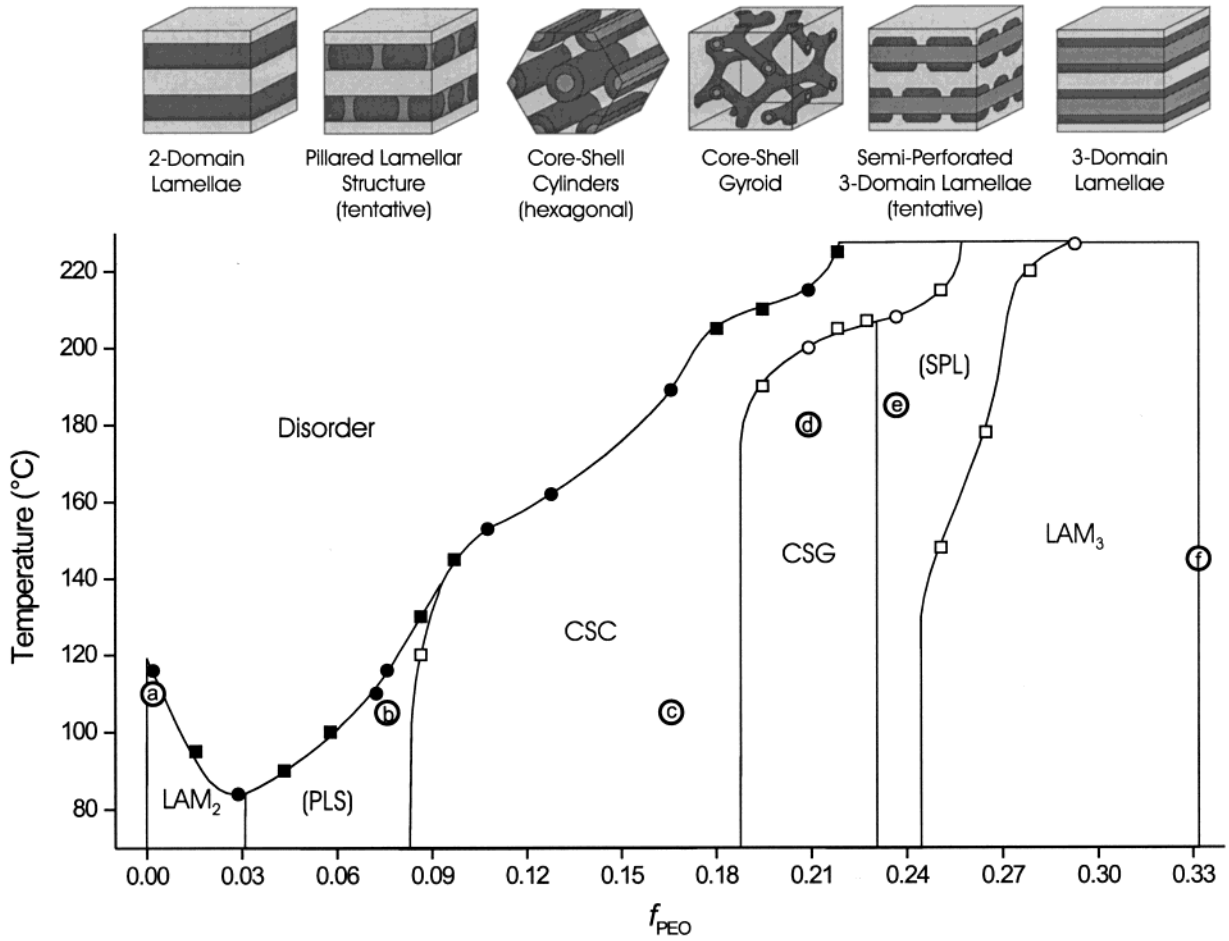

Figure 2. Phase diagram summarizing the morphological behavior of the PS−PI−PEO triblock copolymer system between the symmetric AB and ABC compositional states. (●) and (■) designate ODTs corresponding to neat triblocks and blends of consecutive triblock pairs, respectively. (○) and (□) designate OOTs corresponding to neat triblocks and blends of consecutive triblock pairs, respectively. Circled letters correspond to locations on the phase diagram where SAXS data given in Figures 3−5 were recorded.

SAXS data alone. The vertical boundaries depicted in Figure 2 fall between consecutive samples exhibiting different structural characteristics; however, the specific composition at which each of these boundaries is placed, we note, is arbitrary. In many cases, Bragg reflections in the scattering data were consistent with assignable morphological structures. To complement these data, TEM was used to visualize the melt state morphologies in these samples, when those morphologies could be adequately trapped at room temperature. In all TEM samples, PI domains were selectively stained with OsO_4 to create contrast and supply information about the spatial arrangements of domains within their morphologies.

Using this collection of analytical techniques, we were able to distinguish six different morphologies over this range of phase space. Analysis of example data used to assign each of these morphological regions is discussed in detail below.

Two-Domain Lamellae. This region is defined by data collected from the parent diblock, triblock A, and a symmetric blend of the two, DB/A-1 (Table 2), which collectively represent a composition range between 0 and 3.1 vol % PEO[36] (Figure 2). The original PS−PI parent diblock used was nearly symmetric ($f_{PS} = 0.497$), with an ODT occurring at 116 °C. We note that this molecule was "designed" with the ODT occurring as low as possible in the experimentally accessible window while simultaneously avoiding vitrification effects associated with the PS glass transition ($T_g \cong 100$ °C). In contrast, we did not anticipate the general decrease in the ODT observed as the volume fraction of PEO was increased over this region, although in hindsight this behavior might easily have been predicted. We address this matter in greater detail in the Discussion section that follows. SAXS data for all three samples gave strong first-order reflections; however, higher-order reflections (second, third, and fourth) were noticeably absent in experiments probing higher values of q. Figure 3a contains an example of the scattering data and TEM images associated with these samples, with the particular data presented generated by the parent diblock. TEM confirmed the expected lamellar structure; however, the samples always appeared weakly segregated with domain correlation limited to only several multiples of the principal domain spacing, both perpendicular and parallel to the interfacial plane. This absence of long-range order coupled with the symmetry inherent in these samples supports the absence of higher-order reflections observed in the SAXS data. Considering the formation of a two-domain lamellar structure despite small volume fractions of PEO, it appears the asymmetry in the samples was great enough to suppress segregation into three domains. Instead, the small PEO segments appear to remain mingled within the PI domains. We suspect, however, that preferential seg-

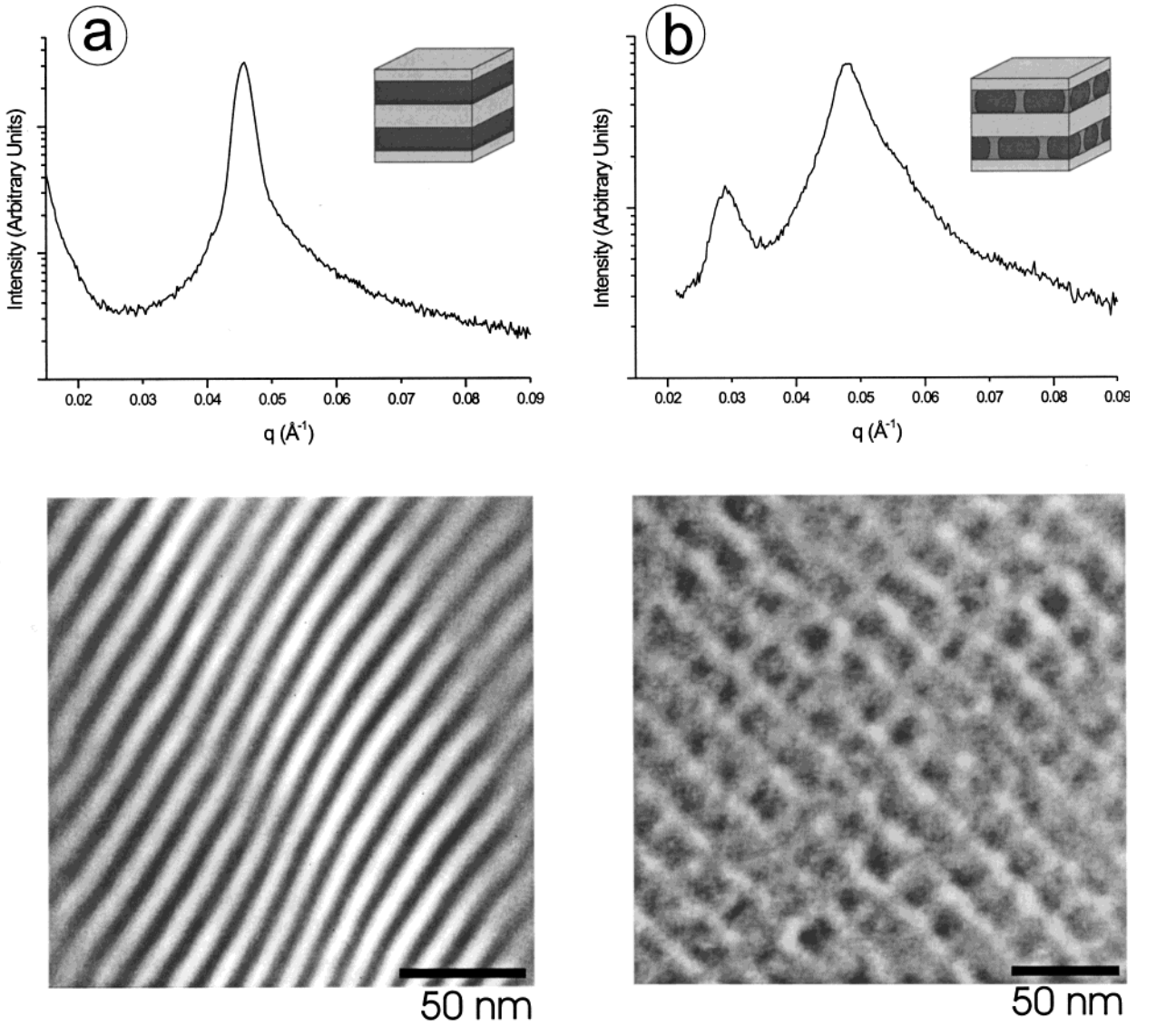

Figure 3. (a) SAXS data (110 °C) and TEM micrograph generated from the parent diblock. Data are representative of the two-domain lamellar region (LAM_2) depicted in Figure 2. (b) SAXS data (105 °C) and TEM micrograph generated from triblock C. Data are representative of the proposed pillared lamellar region (PLS) depicted in Figure 2. Dark regions in TEM micrographs correspond to OsO_4 stained polyisoprene domains. Polystyrene (unstained) and poly(ethylene oxide) (slightly stained) domains appear much lighter (applies to all TEM micrographs of Figures 3−5).

regation within the PI domains is occurring, with PEO segments collecting along the PS interface to reduce enthalpic penalties associated with this two-domain configuration.

Finally, we note that for samples in which the ODT occurs near or below the PS glass transition (triblock A, blends DB/A-1, A/B-1, and A/B-2), growing segregation and structure development is likely retarded by PS vitrification shortly after leaving the disordered state. That we observed only weakly ordered structures by TEM of both the two-domain lamellar and pillared lamellar regions (discussed below) is consistent with the proximity of these two transitions. Higher molecular weight analogues separating the ODT from the PS glass transition will likely yield more conclusive results as to the exact structure of these morphologies.

Proposed Pillared Lamellar Structure. This region is defined by data from triblocks B and C and blends A/B-1, A/B-2, and C/D-1, which collectively represent a composition range between 3.1 and 9.0 vol % PEO.[37] The ODTs for this region reverse the previous trend and begin to rise as the composition of PEO is increased. This rising trend in ODT continues for the remainder of the samples studied, consistent with the increasing molecular weight and a growing enthalpic resistance to disorder. SAXS data for samples in this region all reproduced a similar pattern of two broad peaks occurring at q^* and $1.67q^*$. SAXS data and TEM images generated by triblock C are presented in Figure 3b as representative of samples from this region. We surmise that at these compositions the PEO segments have started to segregate from the PI domains; however, the interfaces dividing these domains may remain diffuse. These broad scattering reflections most likely represent a collection of peaks that are indiscernible at these levels of segregation. TEM images on these samples consistently revealed the rectangular bricklike structure shown in Figure 3b. The domain spacing suggested by the magnitude of the principal scattering vector in the SAXS data was consistent with the layer-to-layer distance between unstained diagonals prevalent throughout the TEM image of Figure 3b. To date, we

have yet to verify the identity of this weakly forming morphology; however, we speculate that the bricklike appearance of the projected morphology is the result of PEO pillars spanning the PI domains sandwiched between PS layers (Figure 3b).

We propose that the formation of such a structure is a result of the frustration arising from PEO's preferred contact with PS as it is expelled from the PI domains. As the PEO composition is increased from that associated with the LAM_2 structure, domains of PEO must necessarily form within the PI to minimize contact between the two. However, the PEO simultaneously retains some benefit from using the PS interface to also shield its contacts with PI. The result is the formation of PEO pillars within the PI domains, which effectively bridge and contact the adjacent PS layers. That the additional PS/PEO interface would form, we argue, is the result of a direct compromise, possible at these compositions, between the architectural requirements and the enthalpic preferences of this system.

We also observed that at the highest composition represented by this region (blend C/D-1, 8.7% PEO) the proposed pillared lamellar structure only occurred over a small range of temperature (between 120 and 130 °C) just prior to disordering. Below 120 °C this blend was found to express the CSC morphology, suggestive of a small area of thermally induced OOTs between these two morphologies.

Hexagonally Arranged Core−Shell Cylinders. This region is defined by data collected from triblocks D, E, F, G, and H as well as blends C/D-1, C/D-2, F/G-1, F/G-2, G/H-1, G/H-2, and H/I-1 (Table 2). These samples represent a composition range of 8.2−25.5 vol % PEO, by far the largest range of composition of any of the morphologies identified in this study. Scattering experiments performed on these samples produced Bragg reflections at wave vectors consistent with a hexagonal arrangement of the PS, PI, and PEO domains, occurring at ratios to the principal scattering vector q^* of $\sqrt{3}$, $\sqrt{4}$, $\sqrt{7}$, $\sqrt{9}$, $\sqrt{12}$, $\sqrt{13}$, and $\sqrt{16}$ (not shown).[38,39] Representative data generated from triblock F are given in Figure 4a. Visualization of this hexagonal structure by TEM confirmed a core(PEO)−shell(PI) cylindrical structure arranged hexagonally in a PS matrix. The layered structure associated with the long axis of the cylindrical morphology was also verified by TEM but has not been included here.

We have mentioned the OOT observed between this CSC morphology and the proposed PLS at the low PEO side of this region. At higher PEO compositions, beyond 18.7%, we found the presence of the CSC morphology limited to a small window of temperatures bracketed above by the disordered phase and below by the CSG and suspected SPL morphologies. SAXS data on samples in this temperature range gave reflections still consistent with a hexagonal arrangement of domains. Scattering was similar to that observed at lower PEO compositions in the region, with the exception of a noticeable reduction in intensity of the $\sqrt{4}$ reflection and a loss of higher-order reflections ($\sqrt{12}$, $\sqrt{13}$, etc.). In our attempts to verify that the spatial domain arrangement in this region was still core−shell, we found trapping of the hexagonal morphology from this bounded channel for investigation by TEM impossible. This was directly a result of the facile nature of the transitions to the other morphologies (CSG and SPL) upon cooling, regardless of the rate. However, in the blend F/G-1 at 17.8% we did observe the reduction in the intensity of the $\sqrt{4}$ peak to occur gradually and continuously as the temperature was increased, and scattering profiles at temperatures just below the ODT were found to closely mimic that observed in the bounded channel. That this blend falls at a composition just on the border of this channel gives us reason to believe that no major rearrangement is taking place. This argument is also supported by the occurrence of an OOT to another core−shell morphology, namely the CSG phase, along the low-temperature side of this channel. We cannot rule out the possibility, however, of significant mixing between two of the domains at these temperatures, resulting in the altered relative scattering intensities and the loss of higher-order peaks.

Pentacontinuous Core−Shell Gyroid. This region is defined by data from triblock G and blends F/G-2, G/H-1, and G/H-2, which collectively represent a composition range between 18.7 and 23.0 vol % PEO. SAXS data and TEM from triblock G are presented in Figure 4b as an example of data typical of this region. The exceptional scattering for this particular system allows assignment of Bragg reflections consistent with the $Ia\bar{3}d$ cubic space group associated with the gyroid and core−shell gyroid morphologies. Ratios of higher-order peak positions to that of the principal scattering vector q^* (in this case $\sqrt{6}$, corresponding to the (211) family of reflections) allow clear assignment of the following major peaks in the experimental data: $\sqrt{8}$, $\sqrt{14}$, $\sqrt{16}$, $\sqrt{20}$, $\sqrt{22}$, $\sqrt{38}$, and $\sqrt{50}$. These correspond nicely with the allowed reflections of the $Ia\bar{3}d$ space group of $\sqrt{8}$, $\sqrt{14}$, $\sqrt{16}$, $\sqrt{20}$, $\sqrt{22}$, $\sqrt{24}$, $\sqrt{26}$, $\sqrt{30}$, $\sqrt{32}$, $\sqrt{38}$, $\sqrt{40}$, $\sqrt{42}$, and $\sqrt{50}$.[38−40]

Although many of the allowed reflections are not observed explicitly, obvious shoulders in the experimental data are consistent with their presence, namely those corresponding to the $\sqrt{24}$, $\sqrt{26}$, $\sqrt{30}$, and $\sqrt{32}$ reflections. Arrows have been used to designate the calculated locations of the unresolvable reflections in Figure 4b. Interestingly, data generated by the morphology in this region show remarkable similarities to that reported by Shelfelbine et al. in their careful assignment of the pentacontinuous core−shell gyroid morphology to a poly(isoprene-*b*-styrene-*b*-dimethylsiloxane) (ISD) ABC triblock copolymer.[4] In fact, the composition of the ISD triblock in which they observed this structure is virtually identical (0.4/0.4/0.2, I/S/D) to the composition of triblock G to which the data in Figure 4b correspond. Importantly, the relationship of the three Flory interaction parameters is also very similar for both systems ($\chi_{BC} > \chi_{AB} \sim \chi_{AC}$). Accordingly, we present a TEM image in Figure 4b which corresponds closely to one presented in the ISD report, where a comparison between their image and one predicted for the [111] projection of the core−shell gyroid morphology using self-consistent-field theory (SCFT) is made. The similarities between our images and those predicted from SCFT are remarkable, when one accounts for the reversal in contrast resulting from the differences in block connectivity in the two ABC systems.

An interesting feature of this region is the line of OOTs defining the conversion of the CSG to CSC morphologies, which invariably preempts the direct disordering of the CSG phase. Although we observed this transition to be a reversible one during slow changes in temperature, a significant degree of hysteresis upon cooling led us to investigate this transition more closely.

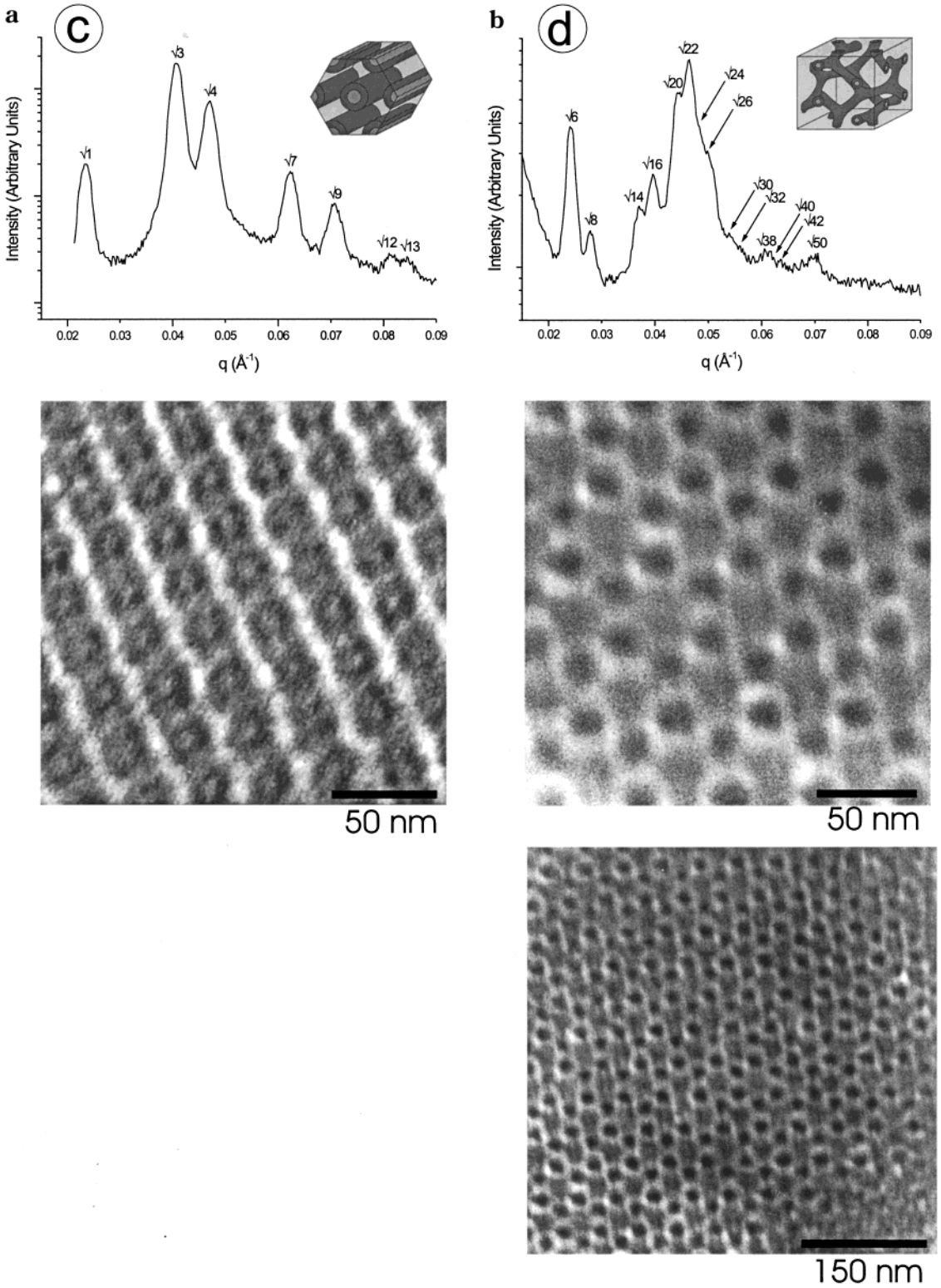

Figure 4. (a) SAXS data (100 °C) and TEM micrograph generated from triblock F. Data are representative of the hexagonally packed core−shell cylinder region (CSC) depicted in Figure 2. Spacing ratios consistent with a hexagonal arrangement have been assigned to reflections in the scattering data. (b) SAXS data (180 °C) and TEM micrograph generated from triblock G. Data are representative of the pentacontinuous core−shell gyroid region (CSG) depicted in Figure 2. Spacing ratios consistent with the cubic $Ia\bar{3}d$ space group have been assigned to reflections in the scattering data. For unobvious reflections, arrows indicate the approximate location those reflections would appear. The TEM micrograph corresponds to the [111] projection of the CSG morphology, in agreement with images previously reported by Shefelbine et al.[4]

A discussion of the reversibility characteristics of this OOT follows at the conclusion of this section.

Suspected Semiperforated Three-Domain Lamellae. Data representing this region are derived from triblocks H and I and blends H/I-1, H/I-2, and H/I-3, which collectively represent a composition range between 23.0 and 29.0 vol % PEO. Scattering reflections exhibited by samples from this region appear at ratios to the principal scattering vector of 1.64, 1.80, 1.97, and 2.93. We have not yet been able to assign these peaks

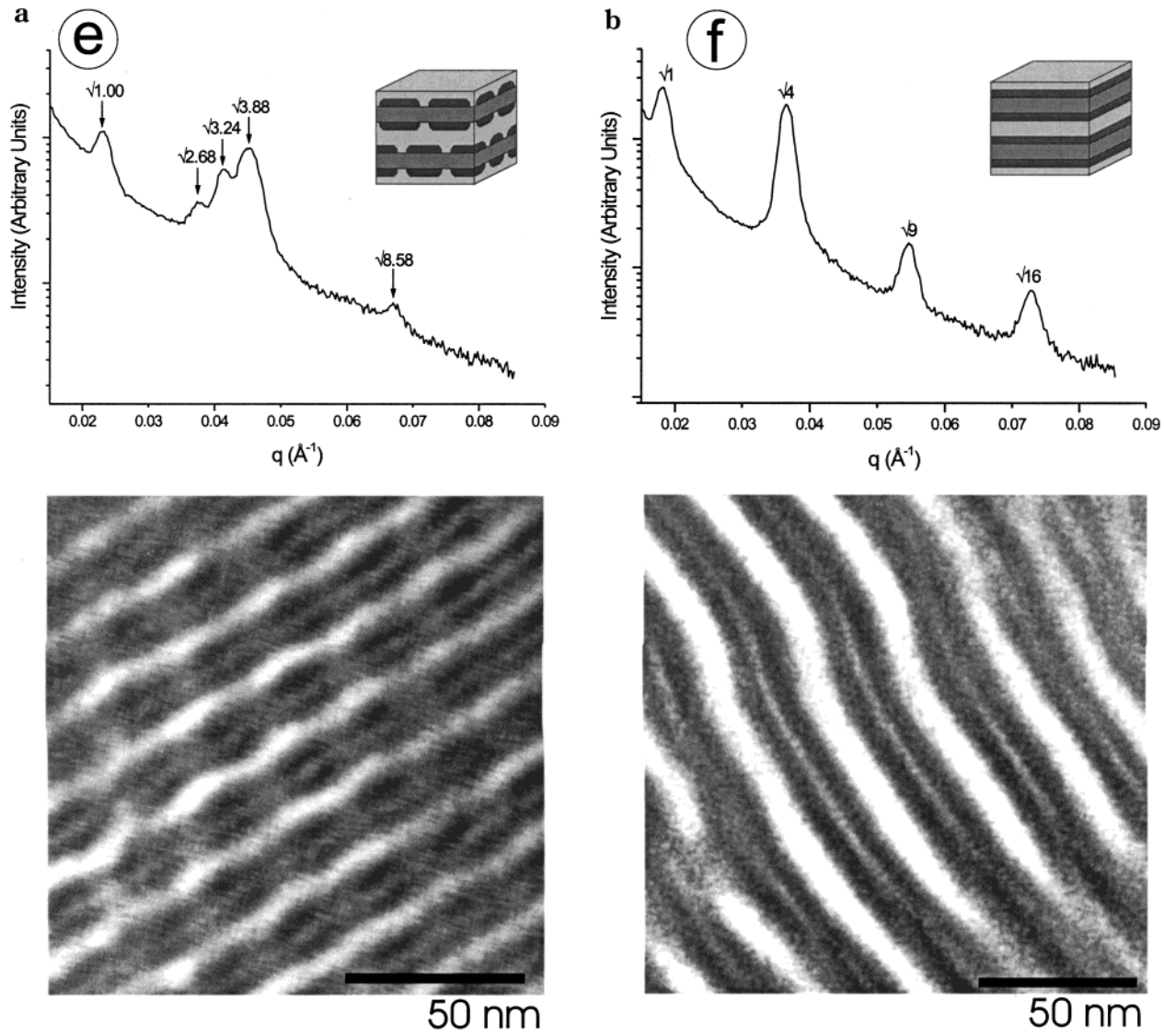

Figure 5. (a) SAXS data (185 °C) and TEM micrograph generated from triblock H. Data are representative of the suspected semiperforated three-domain lamellar region (SPL) depicted in Figure 2. Unassigned spacing ratios have been designated on reflections in the scattering data. (b) SAXS data (145 °C) and TEM micrograph generated from triblock J. Data are representative of the three-domain lamellar region (LAM_3) depicted in Figure 2. Spacing ratios consistent with the lamellar morphology have been assigned to reflections in the scattering data.

to particular reflections of a specific morphology, which might suggest that they represent a morphology with more than one nondegenerate primary length scale. We are particularly intrigued by the characteristic close arrangement of three higher-order reflections which cannot be assigned to integer square-root values relative to the principal scattering vector. This three-peaked feature is evident in the full scattering profile shown in Figure 5a, which in this case was generated from triblock H. Using TEM of this region to help visualize this morphology, we observed only a single consistently reproducible image, an example of which is also depicted in Figure 5a.

We first point out the similarities of the structure captured in this TEM image to the three-domain lamellar structure observed in Figure 5b. Identical sequencing of the repeated layered structure is evident in both images, with the exception of the regularly overlaid, stain diluted "channels" found to bridge the unstained PS and PEO domains. We propose that these diluted regions arise from the formation of perforations in the stained PI layers, which permit periodic contact between PS and PEO domains. Similar to the argument proposed concerning the formation of the pillared lamellar structure, we feel that these perforations result in the formation of a third interface and represent a compromise between the architectural requirements and the enthalpic preferences of this system. We are unable detect from these images whether the perforations represent "holes" in the PI layer or in-plane channels creating disconnected PI lenses organized at the PS/PEO interfaces. Although the latter structure is similar to the *ls* morphology (B spheres at A/C lamellae) previously identified by Breiner et al.,[25] we suspect this morphology would have extreme difficulty accommodating all of the PI volume in our sample. This argument is supported by the large disparity between the composition of the Breiner samples (0.47/0.075/0.455 and 0.45/0.06/0.49) and triblock H (0.380/0.383/0.237) considered here. We are also unable from these micrographs to propose what the intraplane and interplane organization of these perforations might be; however, we acknowledge that a periodic spatial relationship between the perforations is apparent in micrographs of this

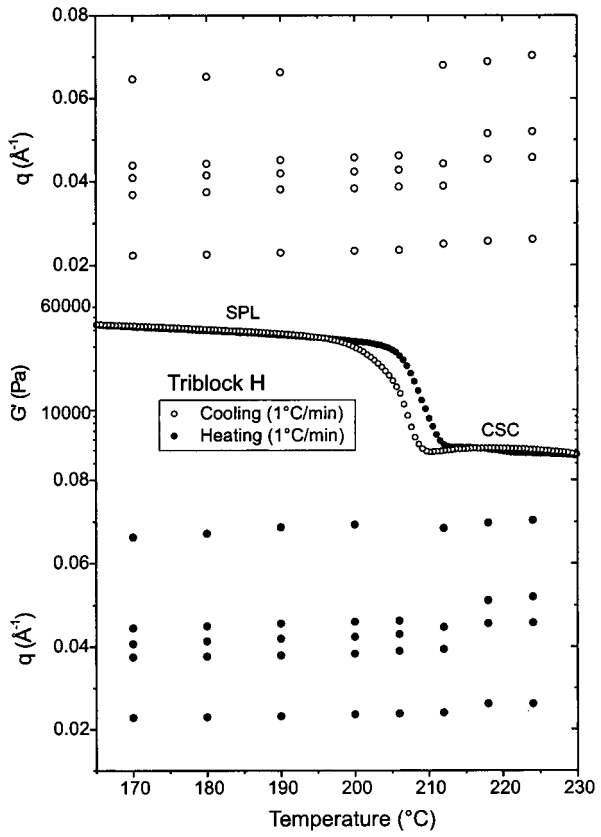

Figure 6. Elastic modulus (G') and scattering reflection positions as a function of temperature for triblock H. Data were recorded while both heating (●) and cooling (○) slowly (1 °C/min) through the OOT between the suspected SPL and CSC morphologies. Note the change of scale occurring in the ordinate axis.

structure. Although we suspect that the unique scattering observed contains information concerning the organization of these perforations, we have yet to make a definitive connection. Given the layered structure suggested by the micrographs, the SAXS peak spacing ratios of 1.00, 1.97, and 2.93 (±0.01) appear related to the expected values (1, 2, 3, ...) for a layered structure.

Like the CSG morphological region, direct disordering of the suspected SPL phase was preempted by an OOT to the CSC morphology.[41] A detailed examination of this OOT by coupling rheology and SAXS data is presented in Figure 6. SAXS data in the figure are plotted simply as a collection of the major peak positions (q values) observed as the temperature of the scattering experiments is varied. Thus, each vertical column of data points represents its own scattering experiment, performed at one specific temperature. Separate experiments were run consecutively, although temperatures were changed stepwise, allowing 10 min of annealing time prior to 6 min acquisition periods at each temperature investigated. Rheological data were collected while changing the temperature continuously, both heating and cooling through the OOT at 1 °C/min. The OOT in this collection of data corresponds to the abrupt change in the elastic modulus of the sample that is observed in both the heating and cooling curves. The SAXS data mimic this change nicely, and the transformation from the three-peaked profile (suspected SPL) to that typical of the hexagonally packed CSC phase ($\sqrt{1}$, $\sqrt{3}$, $\sqrt{4}$, $\sqrt{7}$, ...) is easily distinguishable. Only a small degree of hysteresis (upon cooling) is observed in either the rheology or the SAXS data, which speaks to the facile nature and reversibility of the transition between the CSC and suspected SPL morphologies, regardless of the direction of temperature change. It will be shown below that this is in stark contrast to the transition between the CSG and CSC morphologies, which shows considerable hysteresis and nonequilibrium rate effects in the cooling direction.

That we might see such a morphology dividing lamellar and gyroid phases is not entirely surprising, given its previous appearance between these phases in several AB systems, including the PS−PI system upon which these triblocks are based.[15,19,20] The issue of whether this suspected SPL morphology is in fact an equilibrium structure is an important one, given the theoretically and experimentally proven metastability of the PL phase in AB systems.[33−35] We return to this matter in significant detail at the conclusion of this section; however, we state now our belief that the SPL structure represents an equilibrium morphology over the composition range it has been assigned in the phase diagram of Figure 2.

Three-Domain Lamellae. This final region studied is represented by triblock I and J and blends H/I-1, H/I-2, H/I-3, and I/J-1, which collectively represent PEO compositions above 24.5 vol %. The extent that this region continues beyond the composition of the last triblock in the sequence (33.2 vol % PEO) was not investigated. Data typical of this region are represented in Figure 5b by a SAXS profile and a TEM micrograph taken from triblock J. Scattering reflections for samples in this region were consistent with a three-domain lamellar structure, occurring at integral ratios (1, 2, 3, 4, ...) to the principal scattering vector.[38,39] TEM images also portrayed the lamellar structure and allowed confirmation of the typical head-to-head, tail-to-tail stacking of molecules (...ABCCBA...). The apparent discrepancy between the observed width of the PEO domains and that expected from the compositional symmetry of triblock J is attributed to the densification of PEO below its melt temperature ($T_m \cong 65$ °C), consistent with TEM investigations at room temperature.

Finally, a line of OOTs is established for blends H/I-1, H/I-2, and H/I-3, between the LAM_3 phase and the suspected SPL morphology. In addition, rheological measurements on triblock I also suggested an OOT (denoted in Figure 2); however, the high temperature at which it occurred (225 °C) and the limitations of the SAXS instrumentation prohibited characterization of the event. More detailed investigations of these transitions were not performed, recognizing that the majority of information suggesting the line of OOTs was derived from blended samples. Although we are confident in the use of consecutive pair blends to approximate phase boundaries in this system, extracting more detailed information about the subtleties of OOTs may not be merited. Interestingly, however, the transition from LAM_3 to SPL in these blends appeared to occur gradually with increasing temperature, giving no abrupt discontinuity in the domain spacing. In fact, identification of the transition was based on the slow in-growth of two peaks just inside the $\sqrt{4}$ lamellar reflection (giving the three-peaked feature), and so the exact designation of these transitions in Figure 2 was to some extent subjective.

Hysteresis in the CSG to CSC Order−Order Transition. For most ODTs and OOTs characterizing this system, little hysteresis was detected in transition

temperatures when approaching slowly (1 °C/min) from either above or below the transition. An example of this was discussed in an earlier consideration of the OOT from the suspected SPL to CSC morphology found in triblock H. One notable exception, however, was found in the OOT between CSG and CSC phases in triblock G, where formation of the CSG morphology upon cooling showed significant hysteresis. Rheology and scattering data recorded while heating and cooling through this transition are shown in Figure 7a. As in Figure 6, SAXS data are plotted as a collection of the major peak positions (q values), recorded as the temperature was increased stepwise. Thermal soak times and acquisition times were 10 and 6 min, respectively. Rheological data were collected while changing the temperature continuously, both heating and cooling through the OOT at 1 °C/min. The abrupt changes in elastic modulus upon heating and cooling correspond to the OOT and ODT for this sample. The interesting features in these data are the delayed onset of the transition from CSC to the CSG phase upon cooling and the subsequent slow recovery of the modulus once the transition has occurred. The eventual coincidence of the moduli below the transition region is consistent with a reversible transition; however, the slow recovery of the modulus suggests some inherent resistance to the reformation of the CSG phase. A direct comparison of the scattering and rheology data show the transition to the CSG phase upon cooling begins near the minimum in the elastic modulus. The scattering therefore suggests that the CSG morphology is present beyond this minimum, despite having a reduced modulus over a significant range of temperature. Although it is difficult to assign the causes for the slow recovery of the modulus, we speculate it is related to the complexity of the reorganization process required when starting with the CSC morphology. In fact, the scattering profile at 188 °C, in the region of reduced modulus, shows a prominent peak consistent with the $\sqrt{3}$ reflection of the CSC morphology (Figure 7a). This peak diminishes in intensity by 180 °C, where the modulus has finally obtained the CSG plateau value. Although such hysteresis is often associated with kinetic effects of cooling too rapidly, multiple scattering experiments performed at much slower effective ($\sim$0.1 °C/min) cooling rates gave similar behavior, including the persistence of the $\sqrt{4}$ CSC reflection. Regardless, reorganization from a morphology continuous in only one domain (CSC) to one continuous in all three domains (CSG) is apparently difficult to coordinate on a local scale. The manner in which the dividing surfaces are manipulated to manifest this transformation is a interesting question that is currently without explanation.

Recognizing the hindered manner in which the cooling transition occurred, we decided to investigate the response to very rapid cooling through this transition. The results were dramatic. By quenching ($\cong$ 25 °C/min) samples from the CSC equilibrium state at 210 °C to temperatures below the transition region (180, 175, 165, 160, and 150 °C), all samples avoided initial formation of the CSG phase entirely. Instead, scattering data for all samples gave reflection spacing ratios and the characteristic three-ring pattern typical of the suspected SPL morphology, not previously observed at this PEO composition. Subsequent annealing of these samples at their respective quench temperatures resulted in the eventual conversion of the trapped SPL morphology to the CSG phase for all quench temperatures except 150 °C, verifying the metastability of the SPL morphology at this composition (Table 3). Annealing times required to evoke the SPL to CSG transition appeared exponentially related to the depth of the quench, as is shown in Table 3. Rough estimates based on a two-parameter exponential suggest 35 h would be required at 150 °C, consistent with no change being observed after 12 h of annealing at this temperature.

Figure 7b shows rheology and SAXS data recorded during slow heating of the sample quenched to 150 °C from the ordered CSC state at 210 °C. As before, rheology data were collected while changing the temperature continuously at 1 °C/min, while the temperature in the scattering data was changed stepwise with 10 min thermal soak times and 6 min acquisition periods. Both the elastic and loss moduli are plotted in Figure 7b to emphasize the transition regions. Collection of data during the quench was not possible due to the limited duration of the temperature change. The results of the scattering data taken at 150 °C just after the quench immediately show the profound effect of the rapid cooling rate. The change in morphology from the CSC phase to the suspected SPL morphology has occurred almost instantaneously. Slow heating of the sample from 150 °C resulted in the eventual release of the SPL morphology and subsequent formation of the CSG phase, with this transition occurring around 175 °C. Continued heating resulted in an OOT transition from CSG to CSC at just under 200 °C, in agreement with the behavior observed in other slow heating experiments on this specific triblock (see Figure 7a).

It appears the facile nature of the CSC to SPL transition, demonstrated earlier by data collected on triblock H (Figure 6), allows the SPL phase to supersede the hindered transformation to CSG, when cooling is performed too rapidly. We speculate that the transition from CSC to CSG likely occurs through a rearrangement process that at some point closely resembles the suspected SPL morphology. Consequently, we observe the preferential formation (trapping) of such a structure during very rapid cooling. We hypothesize that, at temperatures near the CSC to CSG transition, the suspected SPL and CSG morphologies are nearly degenerate in free energy, reducing the driving force for conversion to the CSG morphology and allowing the nonequilibrium SPL morphology to persist for long times in a metastable state. Thus, we argue that the preempting of the CSG phase by the suspected SPL morphology is purely a consequence of the extended time scales necessary for coordinated rearrangement to take place. As suggested earlier, further insight into this matter may emerge from theoretical or experimental considerations of the manner in which the dividing surfaces are transformed to effect this particular change in morphology, similar to the discussion by Matsen detailing the cylinder to gyroid transformation observed in AB systems.[42]

Unfortunately, the existence of the SPL morphology in a metastable state at 20.9% PEO (triblock G) questions its existence as an equilibrium morphology at 23.7% PEO (triblock H). The evidence for equilibrium is strongly suggested by the reversibility of the CSC to SPL transition at this composition (Figure 6). To confirm that the SPL morphology detected here was not simply a severe case of preempting of the formation of some other equilibrium morphology, 12 h SAXS annealing experiments were performed at 190 and 200 °C, just

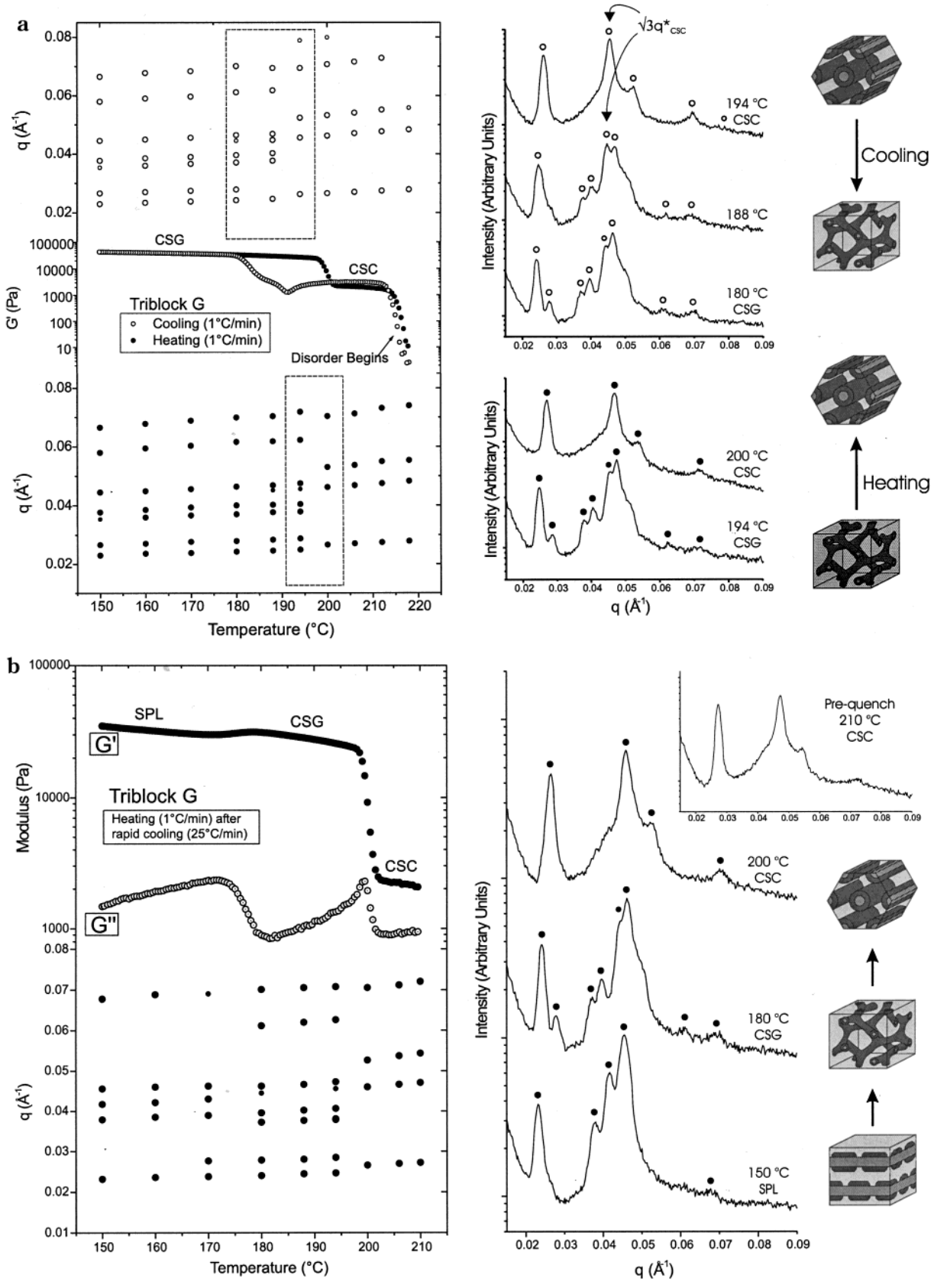

Figure 7. (a) Elastic modulus (*G*′) and scattering reflection positions as a function of temperature for triblock G. Data were recorded while both heating (●) and cooling (○) slowly (1 °C/min) through the OOT between the CSG and CSC morphologies and the subsequent ODT. Note the change of scale occurring in the ordinate axis. SAXS profiles for the cooling and heating transition regions are also presented. Scattering data are sized according to the resolvability of the peaks they represent. (b) Elastic (●) and loss (⊙) moduli and scattering reflection positions for triblock G while heating following a rapid quench (∼25 °C/min) from 210 °C. Data corresponding to the duration of the quench are not shown. SAXS profiles depicting the three ordered morphologies are also presented. Scattering data are sized according to the resolvability of the peaks they represent.

Table 3

quench temp (°C) (from 210 °C)	time to convert from SPL to CSG (min)
180	5
175	9
165	60
160	190
150	no conversion after 12 h

below the transition region. Neither experiment resulted in any deviation of the structure from the SPL morphology. We cannot claim unequivocally that the structure we observe at 23.7% PEO, SPL or not, is an equilibrium morphology. However, we have found no evidence to the contrary.

Discussion

We have presented data describing the existence of six different morphologies found to span the compositionally symmetric AB and ABC states. These include four conclusively defined morphologies (LAM_2, CSC, CSG, LAM_3) and two tentatively assigned morphologies (PLS, SPL) suggested by the current collection of data. While discussing these results, we exploited the concept of a frustration condition, present in ABC systems when block connectivity requires interface formation contrary to that preferred enthalpically. Recognizing that this frustration condition is present in the PS−PI−PEO system, we rationalized the apparent presence of a third (PS/PEO) interface in the two tentatively assigned morphologies. That this additional interface only forms over small regions of composition (Figure 2) is indicative of the predominant role connectivity plays in dictating the spatial arrangement of molecules. It appears that only at particular compositions does the formation of the third interface actually contribute to an overall free energy minimization, and so its formation is not observed over much of the composition range. This can be understood by recognizing the entropic contribution to the overall free energy is directly affected by the chain stretching required to form a third interface, and so actual formation would be contingent on the careful balance between these opposing forces.

In fact, the highly unfavorable PI/PEO interactions of the PS−PI−PEO system described here closely mimic the unfavorable PB/PMMA and PEB/PMMA interactions of the poly(styrene-*b*-ethylene-*co*-butylene-*b*-methyl methacrylate) (SBM) and poly(styrene-*b*-ethylene-*co*-butylene-*b*-methyl methacrylate) (SEBM) systems, in which a diverse collection of morphologies containing A/C interfaces have been identified.[6,9,25] Stadler and coworkers also attribute the formation of such intriguing structures to a desire of these systems to minimize unfavorable B/C block interactions by forming a third more favorable A/C interface. We speculate that, by shuffling the block sequence to remove the frustration condition (PI−PS−PEO, for example), the new system would not form any morphology with more than the required two interfaces over the same range of compositions studied here. Such complementary experiments are under way.

Furthermore, we speculate the frustration condition is also indirectly responsible for the initial decrease in ODT as PEO is added to the parent diblock. Given we only detect two-domain lamellar structures over the relevant composition range, it appears that mixing (partial, at least) of the PEO segments into the PI domain is energetically preferable to a fully segregated state, where large stretching penalties are undoubtedly incurred as a result of large compositional asymmetries in the molecules. Our interpretation of the reduced ODT relative to the parent diblock thus depends on a comparison of the energies associated with the two-domain lamellar structure and the corresponding disordered state.

In the vicinity of the parent diblock ODT, the large value of $\chi_{PI/PEO}$ relative to $\chi_{PS/PEO}$ and $\chi_{PS/PI}$ implies the most significant penalties are incurred for interactions between the PI and PEO segments. PI−PEO contacts are maximized in the two-domain lamellar structure, even if there is significant clustering of PEO chain ends along the PS−PI interface. In contrast, the disordered state allows the PS segments to shield these high-energy PI−PEO contacts, making the transition to the disordered state preferred at reduced temperatures. Although the disordered state also results in many more PS−PI contacts not present in the segregated state, the vicinity of the ODT suggests there is little overall penalty associated with these contacts.

As the percentage of PEO increases, the shielding effect of the disordered state seems to become more advantageous and the ODT continues to decrease. At some composition of PEO, however, diminished compositional asymmetry no longer prohibits the formation of a fully segregated three-domain state. Subsequent to this point, the ODT begins to rise with increasing PEO content. Thus, at small percentages of PEO, large compositional asymmetries force PI and PEO segments to share a single domain, resulting in a comparative energetic advantage for disorder and an associated depression of the ODT.

In addition to this qualitative interpretation, we have performed a RPA stability analysis of this system and have observed a similar decrease (and subsequent increase) in spinodal line, defined as the collection of temperatures at which the scattering structure factor diverges. Similar analysis on the unfrustrated PI−PS−PEO system resulted in a monotonic increase in ODT as PEO was added, consistent with our association of this phenomenon with the specific block sequencing, which forces the unfavorable PI and PEO contacts.

As mentioned at the outset, one of our indirect goals was to locate possible morphologies useful in membrane applications. Beyond the traditional characteristics such as mechanical property tailoring and large internal surface areas intrinsic to block copolymer systems, our motivation was to locate ABC morphologies with multiple domains of isotropic continuity. The additional advantage of such morphologies is the removal of very difficult alignment requirements inevitably necessary for anisotropic structures. Relieving the processing requirements of this potentially tedious and problematic step may be crucial to the imminent use of these materials in practical applications. To date, the gyroid morphology is the only demonstrated ordered morphology possessing a multicontinuous structure,[43] and so defining its compositional range in this PS−PI−PEO system was an important byproduct of this study. Although the amount of experimental work required to prove or disprove the existence of other multicontinuous ordered structures appears to be significant, the requirement of continuity in multiple domains may narrow the regions of phase space in which these structures are likely to occur. We cannot say exactly what defines these regions; however, compositions containing large

asymmetries are most likely to isolate domains in a noncontinuous fashion. There likely exists some minimum composition for each block or pairs of blocks below which continuity becomes unlikely. Molecules with large disparities in block compositions are located at the corners and along the edges of the ternary phase diagram of Figure 1, and so it might be possible to define some internal region within which morphologies would have a higher propensity toward forming multicontinuous domain structures.

One of the most enduring results of the collective work on AB diblock copolymer systems was the establishment of universality in the morphological behavior. It is not clear at present whether the increased complexity of ABC systems will permit any level of generalization to be realized. Not only do the relative ratios of the three interaction parameters have a strong influence on the morphology selected, but for any one system these ratios continuously change given the unique temperature dependence of each interaction parameter. In contrast to this view, however, is the possibility that, like AB systems, there are a finite number of morphologies that ABC systems will adopt. It is also likely that the region of composition in which each morphology is observed will only be associated with a specific area of the ternary composition diagram. Viewed from this perspective, some degree of universality in the behavior of ABC systems seems likely. For example, it is quite possible that in some regions of the composition diagram all ABC systems, regardless of their specific chemistry or interaction parameter ratios, adopt only a single specific morphology. It will be interesting to discover whether the extreme subtleties of each system must be considered or whether a system distinction as simple as frustrated or not frustrated is all that is required to specify the general behavior of an ABC system.

Whether the behavior is universal or not, experimental understanding of ABC systems will undoubtedly require clever strategies to improve the efficiency of these studies. We have taken advantage of some simple functionalization and reinitiation chemistry to reduce the synthetic requirements of the current study. Other innovative uses of chemistry can undoubtedly be taken advantage of to simplify the amount of synthetic work. One possibility might be to adopt a combinatorial approach, synthesizing a series of functional AB diblocks and C homopolymers, followed by systematic coupling, to form a collection of ABC triblock copolymers representing a large range of compositions.

We also have used blending in this study as a means of avoiding additional synthetic efforts and still approximating the behavior in regions falling between compositions of the synthesized molecules. For the current study, we were careful to only blend molecules consecutive in PEO composition, typically separated by only 4 vol %. It should also be noted that because the PS and PI segments of all the molecules are derived from the same parent diblock, the effect of blending was only to increase the polydispersity of the PEO segments. This is a fortuitous byproduct of the synthetic strategy used and is unique to these blending experiments. One source of error that should be considered, however, is a possible change in the preferred curvature of the PI/PEO interface induced by the increased polydispersity in the PEO segments. The proximity in composition of the blended samples (and accompanied small changes in the overall polydispersity), however, undoubtedly minimizes this effect. At any rate, to help confirm the validity of our blending data, we attempted to reproduce the behavior of each triblock by substituting for each a blend of identical composition created from the two triblocks nearest in composition to it. In this case, blends contained molecules with differences in PEO composition of typically 10%; however, the behavior of the triblocks was reproduced by the blends considerably well. The exceptions typically involved small differences in ODT or OOT temperatures or the sharpness exhibited by the scattering profiles. Considering these minor incongruities, we are confident that the blends of consecutive pairs of molecules give reasonably accurate approximations to the true behavior exhibited by this PS−PI−PEO triblock copolymer system.

Finally, the similarities involving the metastability of the PL phase in AB systems and the SPL phase identified in this work are considerable. Hajduk et al.[35] have studied the stability of the PL phase in multiple AB systems, where it is observed in the composition channel falling between the lamellar (L) and cylindrical (C) morphologies, where the gyroid (G) morphology is typically expressed. In the AB samples investigated, the PL phase formed as a metastable state during the *heating* transition from L to G but in all cases converted to G after prolonged isothermal annealing in the transition region. In the PS−PI−PEO system, this behavior is mimicked by the metastable formation of the SPL phase, which forms during the *cooling* transition from CSC to CSG and also converts to CSG after prolonged isothermal annealing. Although the direction of temperature change and the starting morphologies (L and CSC) are different in these two cases, it is clear that the formation of the basic gyroid structure (G and CSG) from other morphologies is inextricably linked with a perforated lamellar-type transient state (PL and SPL).

Conclusion

Using a collection of characterization techniques on a series of PS−PI−PEO triblock copolymers varying only in their PEO content, we were able to determine the approximate phase diagram for intermediate to weakly segregated systems between the symmetric PS−PI and PS−PI−PEO compositional states. Six regions of distinct morphological structure were found to exist within this compositional range. Four of these morphologies—two-domain lamellae, hexagonally packed core−shell cylinders, pentacontinuous core−shell gyroid, and three-domain lamellae—were conclusively assigned. Data for the remaining two morphologies suggested untypical structures containing three distinct interfacial types, We have suggested possible structures in agreement with these data, which we have referred to as pillared lamellar and semiperforated three-domain lamellar structures. Formation of these structures, as well as seemingly anomalous order−disorder transition behavior, is rationalized by the presence of a frustration condition, resulting from block connectivity and χ interaction parameter sequencing in this PS−PI−PEO system.

Investigations into the kinetic reversibility of the core−shell cylinder to core−shell gyroid order−order transition showed complex rate dependence in which trapping of a metastable semiperforated three-domain lamellar structure was possible. This trapped structure is likely the result of a transitional dividing surface that

mimics the semiperforated structure, with the slow transformation to the core−shell gyroid morphology permitting its entrapment. Future studies considering transformation mechanisms between ordered ABC morphologies might be necessary to elucidate a real understanding of transition behavior in these systems. The entangled relationship between the SPL and CSG morphologies reported here is remarkably analogous to the PL and G morphologies of AB systems, with the notable exception of strong evidence suggesting the SPL phase also exists as an equilibrium morphology at other ABC compositions.

Acknowledgment. The authors acknowledge Eric Cochran for his RPA stability analysis and many helpful discussions. This work was supported by the National Science Foundation through Grant DMR-9905008 and the MRSEC at the University of Minnesota, which maintains much of the characterization equipment employed.

References and Notes

(1) Thomas, E. L. *Science* **1999**, *286*, 1307.
(2) Bates, F. S.; Fredrickson, G. H. *Phys. Today* **1999**, *52*, 32−8.
(3) Hueckstaedt, H.; Goldacker, T.; Goepfert, A.; Abetz, V. *Macromolecules* **2000**, *33*, 3757−61.
(4) Shefelbine, T. A. *J. Am. Chem. Soc.* **1999**, *121*, 8457−65.
(5) Breiner, U.; Krappe, U.; Thomas, E. L.; Stadler, R. *Macromolecules* **1998**, *31*, 135−41.
(6) Breiner, U.; Krappe, U.; Jakob, T.; Abetz, V.; Stadler, R. *Polym. Bull. (Berlin)* **1998**, *40*, 219−26.
(7) Brinkmann, S.; Stadler, R.; Thomas, E. L. *Macromolecules* **1998**, *31*, 6566−72.
(8) Breiner, U.; Krappe, U.; Abetz, V.; Stadler, R. *Macromol. Chem. Phys.* **1997**, *198*, 1051−83.
(9) Stadler, R.; Auschra, C.; Beckmann, J.; Krappe, U.; Voight-Martin, I.; Leibler, L. *Macromolecules* **1995**, *28*, 3080−97.
(10) Krappe, U.; Stadler, R.; Voigt-Martin, I. *Macromolecules* **1995**, *28*, 4558−61.
(11) Auschra, C.; Stadler, R. *Macromolecules* **1993**, *26*, 2171−4.
(12) Huckstadt, H.; Gopfert, A.; Abetz, V. *Polymer* **2000**, *41*, 9089−94.
(13) Mogi, Y.; Nomura, M.; Kotsuji, H.; Ohnishi, K.; Matsushita, Y.; Noda, I. *Macromolecules* **1994**, *27*, 6755−60.
(14) Mogi, Y.; Mori, K.; Kotsuji, H.; Matsushita, Y.; Noda, I.; Han, C. C. *Macromolecules* **1993**, *26*, 5169−73.
(15) Bates, F. S.; Schulz, M. F.; Khandpur, A. K.; Foerster, S.; Rosedale, J. H. *Faraday Discuss.* **1995**, *98*, 7−18.
(16) Matsen, M. W.; Bates, F. S. *J. Chem. Phys.* **1997**, *106*, 2436−48.
(17) Hillmyer, M. A.; Bates, F. S.; Almdal, K.; Mortensen, K.; Ryan, A. J.; Fairclough, J. P. A. *Science* **1996**, *271*, 976−8.
(18) Schulz, M. F.; Khandpur, A. K.; Bates, F. S.; Almdal, K.; Mortensen, K.; Hajduk, D. A.; Gruner, S. M. *Macromolecules* **1996**, *29*, 2857−67.
(19) Khandpur, A. K.; Foerster, S.; Bates, F. S.; Hamley, I. W.; Ryan, A. J.; Bras, W.; Almdal, K.; Mortensen, K. *Macromolecules* **1995**, *28*, 8796−806.
(20) Foerster, S.; Khandpur, A. K.; Zhao, J.; Bates, F. S.; Hamley, I. W.; Ryan, A. J.; Bras, W. *Macromolecules* **1994**, *27*, 6922−35.
(21) Hillmyer, M. A.; Bates, F. S. *Macromolecules* **1996**, *29*, 6994−7002.
(22) Bates, F. S. *Science* **1991**, *251*, 898−905.
(23) Flory, P. J. *Principles of Polymer Chemistry;* Cornell University Press: Ithaca, NY, 1953.
(24) Frielinghaus, H.; Hermsdorf, N.; Almdal, K.; Mortensen, K.; Messé, L.; Corvazier, L.; Fairclough, J. P. A.; Ryan, A. J.; Olmsted, P. D.; Hamley, I. *W. Europhys. Lett.*, in press.
(25) **(**25) Breiner, U.; Krappe, U.; Stadler, R. *Macromol. Rapid Commun.* **1996**, *17*, 567−75.
(26) Rosedale, J. H.; Bates, F. S. *Macromolecules* **1990**, *23*, 2329−38.
(27) Hamley, I. W.; Koppi, K. A.; Rosedale, J. H.; Bates, F. S.; Almdal, K.; Mortensen, K. *Macromolecules* **1993**, *26*, 5959−70.
(28) Almdal, K.; Koppi, K. A.; Bates, F. S.; Mortensen, K. *Macromolecules* **1992**, *25*, 1743−51.
(29) Ndoni, S.; Papadakis, C. M.; Bates, F. S.; Almdal, K. *Rev. Sci. Instrum.* **1995**, *66*, 1090−5.
(30) Quirk, R. P.; Ma, J. J. *J. Polym. Sci., Part A: Polym. Chem.* **1988**, *26*, 2031−7.
(31) Morton, M.; Fetters, L. J.; Inomata, J.; Rubio, D. C.; Young, R. N. *Rubber Chem. Technol.* **1976**, *49*, 303−19.
(32) Fetters, L. J.; Lohse, D. J.; Richter, D.; Witten, T. A.; Zirkel, A. *Macromolecules* **1994**, *27*, 4639−47.
(33) Qi, S.; Wang, Z.-G. *Macromolecules* **1997**, *30*, 4491−97.
(34) Qi, S.; Wang, Z.-G. *Phys. Rev. E: Stat. Phys., Plasmas, Fluids, Relat. Interdiscip. Top.* **1997**, *55*, 1682−97.
(35) Hajduk, D. A.; Takenouchi, H.; Hillmyer, M. A.; Bates, F. S.; Vigild, M. E.; Almdal, K. *Macromolecules* **1997**, *30*, 3788−95.
(36) The parent diblock actually contains a single ethylene oxide repeat unit as a result of the functionalization chemistry used.
(37) This range defines compositions at which this morphology has been observed, although it may not be present over the entire temperature range.
(38) Cullity, B. D. *Elements of X-ray Diffraction*, 2nd ed.; Addison-Wesley: Reading, MA, 1978.
(39) *International Tables for X-ray Crystallography*, 3rd ed.; Hahn, T., Ed.; Kluwer Academic Publishers: Boston, MA, 1992.
(40) Hajduk, D. A.; Harper, P. E.; Gruner, S. M.; Honeker, C. C.; Kim, G.; Thomas, E. L.; Fetters, L. J. *Macromolecules* **1994**, *27*, 4063−75.
(41) This may in fact not be true for the entire SPL region; however high-temperature limitations associated with both the polymer system and the SAXS equipment preclude investigation of this matter.
(42) Matsen, M. W. *Phys. Rev. Lett.* **1998**, *80*, 4470−73.
(43) Mogi et al.[13] originally reported the existence of the OTDD morphology; however, these samples have since been reanalyzed and verified to be gyroid by: Matsushita et al. *Physica B* **1998**, *248*, 238−42.

MA0103371